A Thesis

On

Study on multiferroic behaviour of Gd doped $BiFeO_3$ nanoparticles

Submitted in partial fulfillment of the requirement for the award of the degree of

Master of Science (Physics)

Submitted by

Inderdeep Kaur Grewal

Roll No: 300904005

Supervisor

Dr. N. K. Verma

Senior Professor of Physics

Under

School of Physics and Materials Science

Thapar University, Patiala-147 004

July 2011

Dedicated To My

Parents & Teachers

Certificate

This is to certify that the report entitled **"Study on multiferroic behaviour of Gd doped $BiFeO_3$ nanoparticles"** submitted by **Ms. Inderdeep Kaur (300904005)** of **M.Sc (Physics),** Thapar University, Patiala was carried out by her under my supervision. She has not submitted this material for credit towards any other degree at Thapar University, Patiala or any other University.

(Dr. N.K. Verma)

Senior Professor

School of Physics and Materials Science

Thapar University, Patiala

(Dr. O. P. Pandey)

Professor and Head

School of Physics and Materials Science

Thapar University, Patiala

(Dr. S. K. Mohapatra)

Dean of Academic Affairs

Thapar University, Patiala

Acknowledgement

I express my deep sense of gratitude and respect to my guide **Dr. N K Verma, Senior Professor, School of Physics and Materials Science, Thapar University, Patiala** for his keen interest and valuable guidance, strong motivation and constant encouragement during the course of the work. I thank him from the bottom of my heart for introducing me to Nanotechnology. I thank him for his great patience, constructive criticism and many useful suggestions apart from invaluable guidance to me. I am sure that the knowledge gained through my association with my supervisor will help me in future.

I am thankful to **Mr. Gurmeet Singh Lotey** for their kind help and suggestions at every stage of my project report work.

I am also thankful to **Mr. Sanjeev Kumar, Ms. Manveen, Mr. Jaspal Singh, Ms. Lavanya, Mr. Parveen Kumar, Mr. Ravi Shukla** and **my friends** for their help and support at every stage during the project report work.

Finally, I would like to express my deepest gratitude to **my parents,** without whom I am nothing, to provide me great opportunities, everlasting support, big encouragement and lots of love.

Inderdeep Kaur

Inderdeep Kaur

Abstract

Multiferroics defined as materials that exhibit more than one primary ferroic order parameter simultaneously (i.e. in a single phase). The four basic primary ferroic order parameters are ferromagnetism, ferroelectricity, ferroelasticity and ferrotoroidicity. Physics of multiferroics has possible applications in modern optics or in spintronics. They used as memory devices in which magnetic (ferroelectric) domains are controlled by an electric (magnetic) field and magnetooptical devices in which light polarization is controlled by an electric or a magnetic field.

Nanosized rhombohedral structure with hexagonal phase of $BiFeO_3$ nanoparticles doped with Gd were synthesized by solution combustion method using citric acid as fuel. The influence of size and Gd doping on structural, magnetic, ferroelectric and morphological properties have been investigated and tentatively discussed.

The luminescence properties were studied by PL spectra, which confirm the presence of defect levels caused by Gd^{2+}. Magnetic study showed that pure $BiFeO_3$ was antiferromagnetic in nature as no saturation in M-H curve is observed on the other hand Gd doped $BiFeO_3$ is ferromagnetic in nature. The study of ferroelectric behaviour of pure and Gd doped $BiFeO_3$ observed that a weak ferroelectric loop was observed in case of pure and it increased by increasing the doping & 6% Gd doped $BiFeO_3$ show elliptical P-E loop.

List of figures Page No.

Contents Page No.

Chapter 1 Introduction

Christian Oersted's discovery of magnetic field around a current carrying conductor was quite accidental. While Oersted's surprising discovery of electromagnetism paved the way for more practical applications. It was Michael Faraday who gave us the key to relate the electricity and magnetism i.e Electromagnetism which manifests these two fields. Both fields are simply different aspects of electromagnetism, and hence are intrinsically related. In 1865, James Clerk Maxwell proposed four equations governing the dynamics of electric fields, magnetic fields and electric charges, which are now known as Maxwell's equations. They show that magnetic interactions and motion of electric charges, which were initially thought to be two independent phenomena, are intrinsically coupled to each other. In the covariant relativistic form, they reduce to just two equations for the electromagnetic field tensor, succinctly reflecting the unified nature of magnetism and electricity [1]. In a solid, electric field (E) and magnetic field (H) induce electric-polarization (P) and magnetization (M), yet the coupling between M and P is a highly non trivial issue. The coupling, if realized, will enable the magneto electric (ME) affect, namely the mutual control of magnetism and electricity that is M is induced by E, and conversely P by H [2].

Magnetic nanostructures pose experimental challenges, exhibit interesting physical phenomena, and have many present or potential applications. During the last decade Nanocrystalline materials have emerged as new building blocks for magneto electric device applications. The ferromagnetic and ferroelectric properties of solids have been exploited for over a century for various device applications. However, significant achievements in the area of Giant Magneto Resistance (GMR) applications, both in laboratory and technological fronts notably by Peter Grunberg & Albert Fert revolutionarised the minds of researchers to quest for suitable material for read and write head memory devices. It is further felt necessary to enhance or induce ferromagnetism in certain specific advanced and promising materials like diluted magnetic semiconductor, magnetoelectric, multiferroic materials, which have got tremendous applications in future spintronic as compared to existing GMR devices.

1. Multiferroics

In the quest of searching more efficient futuristic multifunctional electronic materials for device applications, it is felt by researchers to couple different properties within one material, which can suitably be tailored for the use of specific devices. Coupling of certain properties like ferromagnetism, ferroelectricity, ferroelectricity, etc. result in the fabrication of multiferroics. Schmid [3] first coined the term 'multiferroic' in 1994. According to original definition, a single-phase multiferroic material is one that possesses at least two of the 'ferroic' properties such as ferroelectricity, ferromagnetism, or ferroelasticity. These materials are attracting increasing interest and provoking much research activity by profound physics of these materials, the coexistence and coupling of 'ferroic' orders, and find wide applications in novel multifunctional fields of 'Spintronic', memories, sensors, transducers relying on magnetoelectric coupling [4]. Thus the research interests increased many fold, in recent years, to couple these properties within a single phase material especially for spintronic applications.

Since its discovery less than one century ago, the phenomenon of ferroelectricity, like superconductivity, has been considered, In relation to the ancient phenomenon of magnetism. Just as recent work has shown that magnetic order can create super-conductivity, it has also been shown that magnetic order can create (weak) ferroelectricity and vice versa. The single-phase materials in which ferromagnetism and ferroelectricity arise independently also exist, but are rare. As this new century unfolds, the study of materials possessing coupled magnetic and electrical order parameters has been revitalized. Multiferroics formally defined as materials that exhibit more than one primary ferroic order parameter simultaneously (i.e. in a single phase). The four basic primary ferroic order parameters are ferromagnetism, ferroelectricity, ferroelectricity and ferrotoroidicity. Moreover, the classification of a multiferroic has been broadened to include anti-ferroic order on the other hand, the coupling between magnetic and (ferro) electric order has long been known as the magnetoelectric (ME) effect, which is the induction of magnetization by an electric field or the induction of electric polarization by a magnetic field. There are very few single-phase ME materials, and most of them show very weak ME coupling at room temperature.

Magnetoelectric multiferroics is an old but emerging class of materials that combine coupled electric and magnetic dipole order. The interaction leads to a so called magnetoelectric effect. The research for these materials is driven by the prospect of controlling charges by

applied magnetic fields and spins by applied voltages, and using this to construct new forms of multifunctional devices. Physics of multiferroics has possible applications in modern optics or in spintronics. They used as memory devices in which magnetic (ferroelectric) domains are controlled by an electric (magnetic) field and magneto-optical devices in which light polarization is controlled by an electric or a magnetic field. From the current search for novel multifunctional materials for next generation electronic devices that explore the control of the magnetic (spin) state via electric field and/or vice versa, with potential for spintronic devices, solid-state transformers, high sensitivity magnetic field sensors, and electromagnet optic actuators.

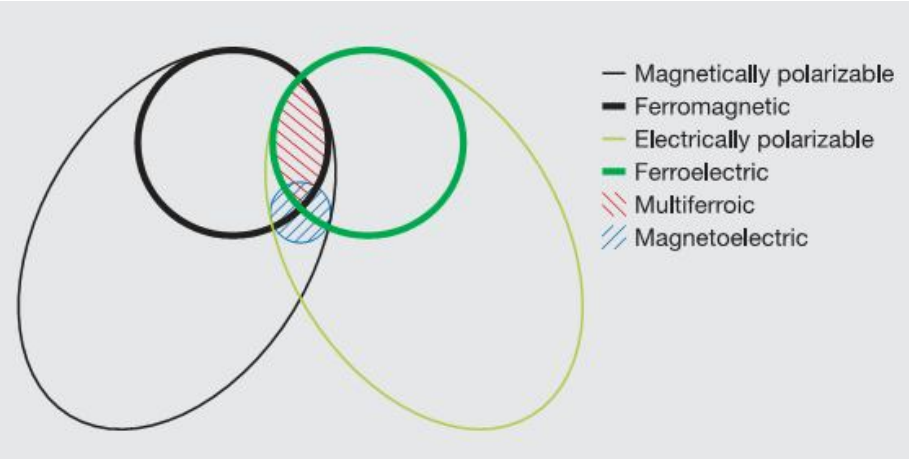

Figure 1.1: The relationship between multiferroic and magnetoelectric materials. Ferromagnets (ferroelectrics) form a subset of magnetically (electrically) polarizable materials such as paramagnets and antiferromagnets (paraelectrics and antiferroelectrics).The intersection (red hatching) represents materials that are multiferroic. Magnetoelectric coupling (blue hatching) is an independent phenomenon that can, but need not; arise in any of the materials that are both magnetically and electrically polarizable [30].

In the next generation of spintronics devices, this should combine memory and logical functions and promises to set new standards in future information technology. The incorporation of multiferroic materials in the field of spintronics should allow one to take advantage of both functionalities (for example, ferromagnetism and ferroelectricity) independently but also to add new functionalities due to the coupling between the two orders. This magnetoelectric coupling between magnetism and ferroelectricity opens the way to control of the polarization by a

magnetic field or that of the magnetization by an electric field. This coupling offers interesting perspectives for the design of ferroelectric memories with a non-destructive magnetic reading or magnetic random access memories (MRAM) with an electrical writing procedure (MERAM).

1.2. Types of Multiferroics

The four main approaches are adopted to make better magneto electric materials.

1.2.1 Lone pair multiferroics

In usual perovskite-based ferroelectrics like $BaTiO_3$, the ferroelectric distortion occurs due to the displacement of B-site cation (Ti) with respect to the oxygen octahedral cage. Here the transition metal ion (Ti in $BaTiO_3$) requires an empty d shell since the ferroelectric displacement occurs due to the hybridization between Ti 3d states and O 2p states. This normally excludes any net magnetic moment because magnetism requires partially filled d shells. However the partially filled d shell on the B-site reduces the tendency of perovskite to display ferroelectricity. In order for the coexistence of magnetism and ferroelectricity (multiferroic), one possible mechanism is lone-pair driven where the A-site cation drives the displacement and partially filled d shell on the B-site contributes to the magnetism. Examples include $BiFeO_3$, $BiMnO_3$, $PbVO_3$ [5]

1.2.2 Charge ordered multiferroics

Charge ordering in the manganates is interesting because charge ordering is resulting due to localization of charges therefore it is associated with insulating and antiferromagnetic (or paramagnetic) behavior. But double exchange gives rise to metallicity along with ferromagnetism. Therefore a competition arises between ferromagnetic metallic and charge ordered antiferromagnetic insulating states. Charge ordering can occur in compounds containing ions of mixed valence with geometrical or magnetic frustration. Example for a charge ordered multiferroics $LuFe_2O_4$, which shows improper ferroelectricity below 330K and ferromagnetic behavior occurs below 240K [5].

1.2.3 Geometrically frustrated multiferroics

Geometric frustrated multiferroicity is related to a structural phase transition at high temperature. Compounds belong to this important class of multiferroics is K_2SeO_4, Cs_2CdI_4 and hexagonal $RMnO_3$. These systems are prototypical multiferroics which can be understood by competition between local interactions in several ion sites. Physical properties of geometric multiferroics are

dominated by the behavior of d-shell electrons of the transition metal ions and unfilled f-shell of the rare earth ions [5].

1.2.4 Magnetically driven ferroelectric multiferroics

Magnetically driven multiferroics are insulating materials, mostly oxides, in which macroscopic electric polarization is induced by magnetic long range order. A necessary but not sufficient condition for the appearance of spontaneous electric polarization is the absence of inversion symmetry. In these materials inversion symmetry is broken by magnetic ordering. Such a symmetry breaking often occurs in so called frustrated magnets, where competing interactions between spins favor unconventional magnetic orders [5].

1.3 Why there are so few multiferroics?

By definition, for a material to be a magneto electric multiferroic, it must be simultaneously ferromagnetic and ferroelectric. Therefore, it's allowed physical, structural, and electronic properties are restricted to those which occur both in ferromagnetic and in ferroelectric materials. In this section, we analyze a range of properties and discuss how these limit our choice of potential multiferroic materials. Using density functional theory (DFT) calculations, we show that the conventional mechanism driving ferroelectricity in perovskite structure oxides requires vacant d orbitals on the small B cation. In contrast, occupied d orbitals are required in order to have any kind of magnetic ordering. Therefore, the coexistence of magnetism and ferroelectricity should in fact never be expected [5].

1.3.1 Symmetry

A primary requirement for the existence of ferroelectricity is a structural distortion from the prototypical high-symmetry phase that removes the center of symmetry and allows an electric polarization. There are 31 point groups that allow a spontaneous electric polarization, P, and 31 that allow a spontaneous magnetic polarization, M. Thirteen point groups are found in both sets, allowing both properties to exist in the same phase. Although this represents a considerable reduction from the total number of possible crystal structures, it is not an insignificant number, and symmetry restrictions are not primarily responsible for the scarcity of ferromagnetic ferroelectric materials.

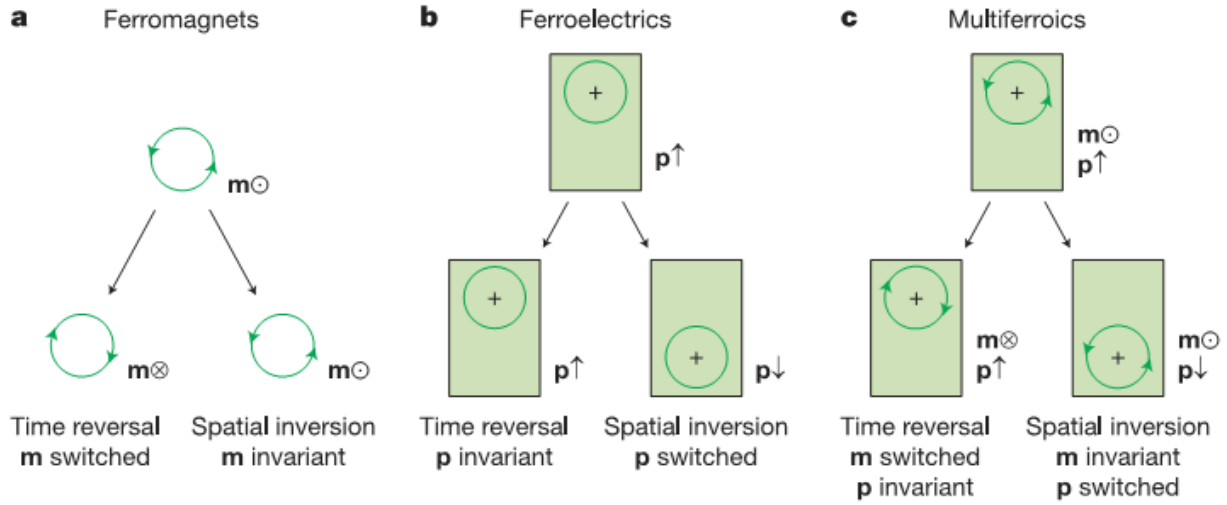

Figure 1.2: The time-reversal and spatial-inversion symmetry in ferroics.

a, The local magnetic moment m may be represented classically by a charge that dynamically traces an orbit, as indicated by the arrowheads. A spatial inversion produces no change, but time reversal switches the orbit and reverses m (magnetic moment).

b, Ferroelectrics. The local dipole moment p may be represented by a positive point charge that lies a symmetrically within a crystallographic unit cell that has no net charge. There is no net time dependence, but spatial inversion reverses p (electric moment)

c, Multiferroics that are both ferromagnetic and ferroelectric possess neither symmetry [5].

1.3.2 Electrical properties

A ferroelectric material must be an insulator (otherwise an applied electric field would induce an electric current to flow, rather than cause an electrical polarization). Ferromagnets, although not required to have specific electrical properties, are often metals. Therefore, one could assume that the lack of simultaneous occurrence of magnetic and ferroelectric ordering is simply the result of a dearth of magnetic insulators. However, if we extend our search to include ferrimagnets or weak ferromagnets, this argument no longer holds because most ferrimagnets or weak ferromagnets are, in fact, insulators. In addition, there are also very few antiferromagnetic ferroelectrics, even though antiferromagnets are usually insulating materials. Therefore, we cannot blame the lack of magnetically ordered ferroelectrics simply on a shortage of magnetically ordered insulators [5].

1.3.3 Chemistry: "d^0-ness"

The common perovskite oxide ferroelectric materials have a formal charge corresponding to the d^0 electron configuration on the B cation. Clearly, if there are no d electrons creating localized magnetic moments, then there can be no magnetic ordering of any type, either ferro, ferri, or antiferromagnetic. It appears however that, in most cases, as soon as the d shell on the small cation is partially occupied, the tendency for it to make a distortion that removes the center of symmetry is eliminated. This could be the result of a number of effects, including size, the tendency to undergo a different, more dominant distortion, electronic properties, magnetic properties, or some combination of the above [5].

1.3.4 Size of the Small Cation

The transition metal ions with occupied d shells simply too large to move away from the large space at the center of the oxygen octahedron. In this section, we compare the ionic radii of typical d^0 cations in perovskite ferroelectrics with those of typical d^n cations in non-ferroelectric perovskite oxides to see if this argument is correct. The Shannon ionic radii of some common d^0 small cations found in ferroelectric perovskite oxides are: Ti^4, 74.5pm; Nb, 78pm and Zr, 86pm. Some representative d^n cations that are found as the small cations in non ferroelectric perovskite oxides include Mn^3 (d^4), Ti^3 (d^1), and V^4 (d^1) with radii of 78.5, 81, and 72pm, respectively. Therefore, typical B-site cations with d electron occupation do not have systematically larger radii than typical d^0 B-site cations. We conclude that the size of the B cation is not the deciding factor in the existence or otherwise of ferroelectricity [5].

1.3.5 Structural Distortions

Ferroelectric materials must undergo a phase transition to a low-temperature phase that does not have a center of symmetry. This is most often achieved in conventional perovskite ferroelectrics by an off-center displacement of the small (B) cation from the center of the oxygen octahedron. However, for cations with certain d-orbital occupancies, the tendency to undergo a Jahn Teller distortion is strong and will likely be the dominant structural effect. The Jahn Teller distorted structure might have a lower driving force for off-center displacement than the otherwise undistorted structure. Examples of this effect are seen in lanthanum manganite, $LaMnO_3$, in which the Mn^3 ion has a d^4 configuration, and yttrium titanate, $YTiO_3$, in which the Ti^3 ion is d^1 [5].

But the scarcity about the multiferroics is that they are rare in nature [12, 27]. Rare materials of these kinds are $BiFeO_3$, $DyFeO_3$, $GdMnO_3$, $Ni_3B_7O_{13}I$, and some compounds like $RMnO_3$,

RMn_2O_3 where R is rare earth metal ions [13]. $BiFeO_3$ is one such few materials [14] having an antiferromagnetic behaviour with a relatively high Néel temperature (T_N=370 °C) and ferroelectric behaviour with a high Curie temperature (T_C=810 °C) [15] and possesses a rhombohedral distorted perovskite structure.

Chapter 2 Review of Literature

The literature was reviewed in detail, in order to gain and gather optimum information as to the genesis and the technical applications of the work and is given as follows:

The magnetoelectric effect was proposed by Curie in 1894 [7], but experimental confirmation of the effect remained elusive until work on Cr_2O_3 in the 1960s [8, 9]. Since the observation by Smolensky et al. [10] in 1958, three different classes of multiferroic systems could be identified—$RMnO_3$ (where R =Dy, Tb, Ho, Y, Lu, etc.), RMn_2O_5 (where R =Nd, Sm, Dy, Tb), and $BiBO_3$-type (where B=Mn, Fe). Such systems depict magnetoelectric coupling and, therefore, magnetic polarization can be achieved by electric field and vice versa. As early as the 1970s a wide range of devices, including devices for the modulation of amplitudes, polarizations, and phases of optical waves, magnetoelectric data storage and switching, optical diodes, spin-wave generation, amplification, and frequency conversion had been proposed that would take advantage of magnetoelectric materials .

But the scarcity about the multiferroics is that they are rare in nature [5, 12, 27]. The perovskite $BiFeO_3$ was first produced in the late 1950s [18] and many of the early studies were focused on the same concepts, important which even today find potential for magnetoelectric coupling [19]. During the 1980s, the magnetic nature of BFO was studied in detail. Early studies indicated that BFO was G-type antiferromagnets with a Neel temperature of 673 K [25] and possessed a cycloidal spin structure with a period of 620A˚ [26].

Hill *et al.* [27] reviewed the density functional theory used both in explaining the properties of known magnetically ordered ferroelectric materials, and, in predicting, the occurrence of new ones. This study showed that Bi compounds will be good candidates for magnetoelectric multiferroism [14]. Although many researchers anticipated strong magnetoelectric coupling in BFO, until the first evidence for this coupling in 2003 by Ramesh group [28]. The unexpectedly large remnant polarization with large ferromagnetism than bulk counterpart has been reported. The observed enhancement is corroborated by first principle calculations and found to originate from small changes in lattice parameters.

Eerenstein *et al.* [29] present relationship between multiferroic and magnetoelectric materials. The magnetoelectric coupling study on single and double phase has been done. Rao et al. [30] explained cause of magnetoelectric coupling in $RMnO_3$, RMn_2O_5, $RCrO_3$, $R_{1-x}Ca_xMnO_3$, and bismuth based compounds. The study on magnetoelectric coupling in multiferroic complex oxide discussed in Vaz et al. [31]. Catalan et al. [32] described the physics, applications and phase transition of $BiFeO_3$.

Mathe *et al.* 2002 [33] synthesized the $Bi_xLa_{1-x}FeO_3$ (x = 0.0, 0.20, 0.40, 0.60, 0.80) by solid-state reaction method. The single-phase formation of these compounds was found. The samples up to x = 0.60 were orthorhombic while the sample with x = 0.80 has changed to triclinic. The dielectric constant (ε) and dissipation factor (tan δ) were measured in the frequency range 100Hz to 1MHz at room temperature and as a function of temperature at certain fixed frequencies (1 kHz, 10 kHz, 100 kHz, 1 MHz). All the samples showed dielectric dispersion. The dielectric constant with temperature shows a broad peak; the peak temperature shifts with frequency which reflects the relaxor-type behavior. The peak above 600K in the measured temperature range corresponds to antiferromagnetic ordering temperature (Neel temperature). The broadness of the peak changes with composition.

Palkar *et al.* 2004 [34] synthesized the $Bi_{0.9-x}TbxLa_{0.1}FeO_3$ powder samples ($0.0<x<0.30$) were developed by using a novel wet chemical route. The coexistence of ferroelectricity and magnetism was found. The samples found to exhibit high RT dielectric constant and magnetoelectric coupling.

Pradhan *et al.* 2005 [35] synthesized single phase $BiFeO_3$ by rapid liquid-phase sintering technique. The temperature-dependent magnetic measurement indicated RT antiferromagnetic behavior in $BiFeO_3$. Although saturated ferroelectric hysteresis loops were observed in single-phase $BiFeO_3$ ceramic synthesized at 880°C, the reduced polarization is found to be due to the high loss and low dielectric permittivity of the ceramic, which is caused by higher leakage current.

Kim *et al.* 2005 [36] synthesized the high purity multiferroic $BiFeO_3$ (BFO) powders by sol–gel process using bismuth nitrate and iron nitrate as sources. The thermal annealing was carried out in N_2 atmosphere. The rhombohedral $BiFeO_3$ phase (R-phase) with a minor impurity phase of Bi_2O_3 is achieved. It is reported that pure BFO R-phase can be obtained by leaching out the minor Bi_2O_3 phase using diluted nitric acid. A reversible phase transformation of the BFO R-

phase has been detected at 836^0C by a differential thermal analysis. The powder of BFO R-phase exhibits a uniform feature with the particle size of 200 nm. The dielectric constant of the BFO R-phase is measured to be ~15 in the frequency range of 104-106 Hz at room temperature.

Wang *et al.* 2006 [37] synthesized Ba substituted $BiFeO_3$ by solid-state reaction method. The substituted samples exhibit magnetism and ferroelectricity simultaneously at room temperature. The magnetoelectric coupling was evidenced by the increase of the dielectric constant with the increase of the applied magnetic field.

Fanggao *et al.* 2006 [38] synthesized $Bi_{1-x}Gd_xFeO_3$ (x = 0.0, 0.05, 0.10, 0.15, 0.20) ceramics by conventional solid state reaction method. Frequency dependence of dielectric properties of $Bi_{1-x}Gd_xFeO_3$ samples at room temperature was measured in a frequency range from 100 Hz to 1MHz.It is found that both dielectric constant and dielectric loss are strongly dependent on the Gd^{3+} content. The effect of introducing Gd^{3+} is to increase the dielectric constant and to decrease the dielectric loss for slightly doped sample $Bi_{0.95}Gd_{0.05}FeO_3$ the dielectric constant of the sample at 1 kHz reaches 600, six times higher than that for pure $BiFeO_3$. Complicated dielectric behaviors are observed at higher doping levels. Furthermore, the substitution of rare earth Gd for Bi helps to eliminate the impurity phases in $BiFeO_3$ ceramics. There is strong evidence that both lattice constants *a* and *c* of the unit cell become smaller as the Gd^{3+} content is increased. The dielectric constant and loss and their frequency responses can be varied dramatically by substitution of Gd.

Khomchenko *et al.* 2007 [39] sintered the $Bi_{1-x}A_xFeO_3$ ceramics (A=Ca, Sr, Pb) by conventional mixed oxide route. The crystallographic structure of all samples is characterized by the rhombohedral symmetry. The existence of switchable ferroelectric polarization is verified by piezoresponse force microscopy. Magnetic properties of Ca and Sr- doped ceramics are found to reproduce the antiferromagnetic behavior of undoped $BiFeO_3$ without any enhancement of the magnetization. On the contrary, Pb-doped compound demonstrates appearance of a weak ferromagnetism. It is thus shown that Pb doping of $BiFeO_3$ is a promising way for preparing multiferroic materials.

Das *et al.* 2007 [40] investigated the magnetic and the electrical properties in lanthanum (La)-modified bismuth ferrite ($Bi_{1-x}La_xFeO_3$, x=0.05, 0.1, 0.15, and 0.2) and compared with undoped bismuth ferrite ($BiFeO_3$). The presence of a small secondary phase of $BiFeO_3$ (arises due to excess Bi_2O_3) was removed on La substitution at the Bi site, as observed in x-ray

diffraction (XRD). The effect of La substitution on dielectric constant, loss tangent, and remnant polarization of the samples was studied in a wide range of temperature (77K–400K) and frequency (1kHz–1MHz). The variation of magnetization, coercive field, with temperature (2K–300K) and La concentration were investigated. These changes in the magnetic parameters with La doping along with those of the electron magnetic resonance parameters measured at 300 K and 9.28GHz are understood in terms of increase in the magnetic anisotropy and magnetization. These results also show that stabilization of crystal structure and non-uniformity in spin cycloid Structure by La substitution enhances the multiferroic properties of $BiFeO_3$.

Su *et al.* 2007 [41] synthesized the $BiFeO_3$ ceramics by sol-gel method (BFO-1) and high-pressure synthesis (BFO-2). X-ray diffraction showed that these ceramics are almost of single phase. It is difficult to observe a ferroelectric loop of BFO-1 even at an electric field of 6kV/cm. Compared to BFO-1, the high-pressure synthesized one has higher resistivity, higher density, and better crystallization. Under an applied electric field of 120kV/cm, the values of remnant polarization and the coercive field are 46μC/cm^2 and 73kV/cm, respectively. At room temperature, a magnetic hysteresis loop with enhanced magnetization was observed in BFO-2.

Thrall *et al.* 2008 [42] synthesized the multiferroic $BiFeO_3$ by using both vacuum and argon atmospheres. The synchrotron X-ray powder diffraction investigation on pressed pellets of the starting powders of Bi_2O_3 and Fe_2O_3 were carried out up to the final formation of $BiFeO_3$. The difference in the transformation temperature of monoclinic Bi_2O_3 to cubic Bi_2O_3 was found to be 650^{0}C and 700^{o}C when samples were sintered in a vacuum and argon environments, respectively. In both cases it was found that the quantity of Fe_2O_3 was unaffected by increasing temperature until after the transition of monoclinic to cubic Bi_2O_3 had reached its maximum value. After this transition the quantities of cubic Bi_2O_3 and Fe_2O_3 were found to decrease at very similar rates yielding the final $BiFeO_3$ structure.

Khomchenko *et al.* 2008 [43] studied the room-temperature crystal structure, local ferroelectric, and magnetic properties of the $Bi_{1-x}Gd_xFeO_3$ (x=0.10, 0.20, 0.30) polycrystalline samples by x-ray diffraction, piezoresponse force microscopy, and magnetometry techniques. Performed measurements have revealed a sequence of the composition-driven structural phase transitions R3c→Pn21a (occurs at x=0.10) and Pn21a→Pnma (takes place within the concentrational range of 0.20<x<0.30). The latter structural transformation is attributed to the substitution-induced suppression of the polar displacements. Gd substitution has been shown to

effectively induce the appearance of the spontaneous magnetization, thus indicating a promising way for improving multiferroic properties

Reddy *et al*. 2009 [44] reported that room temperature spontaneous magnetization and dielectric anomaly at Neel temperature are observed in 15% Eu doped bismuth ferrite indicating the multiferroic nature of the sample. With 15% Eu doping structural transformation from rhombohedral to triclinic is observed. Fe^{3+} and Eu^{3+} oxidation states are observed from 57Fe and 151Eu Mossbauer measurements, respectively. The high field 57Fe Mossbauer spectrum in longitudinal geometry shows an enhancement in the intensity of lines corresponding to m=0 transitions, i.e., second and fifth lines in six line pattern. This observation suggests that the origin of spontaneous magnetization is due to weak ferromagnetism.

Khomchenko *et al.* 2009 [45] studied the crystal structure, magnetic and local ferroelectric properties of polycrystalline $Bi_{1-x}Gd_xFeO_3$ (x = 0.10, 0.20, 0.30) samples at room temperature. Gadolinium substitution was found to induce a polar-to-polar R3cPn21a structural phase transition at x=0.10. Increasing the content of the substituting element suppressed the spontaneous polarization in $Bi_{1-x}Gd_xFeO_3$, resulting in a ferroelectric–paraelectric Pn21a to Pnma phase transition up to the level $0.20 < x < 0.30$. The substitution caused the appearance of a weak ferromagnetic moment.

Simoesa *et al.* 2009 [46] Lanthanum-modified bismuth ferrite ceramics, $Bi_{1-x}La_xFeO_3$ (BLFO), with x ranging from 0.0 to 0.30 were obtained using a polymeric precursor solution. Increasing lanthanum content leads to lower leakage current density and superior ferroelectric hysteresis loops at room temperature.

Al-Haj *et al.* 2010 [47**]** synthesis the multiferroic compounds $Bi_{0.9}Sm_{0.1}FeO_3$, $Bi_{0.9}Gd_{0.1}FeO_3$, $Bi_{0.9}Ca_{0.1}FeO_3$, $Bi_{0.9}Sm_{0.05}Ca_{0.05}FeO_3$, and $Bi_{0.9}Gd_{0.05}Ca_{0.05}FeO_3$ by the conventional ceramic method and were characterized by X-ray diffraction, vibrating sample magnetometry, and differential scanning calorimetry. The compounds were found to have the rhombohedral perovskite-like structure, accompanied by a small residual $Bi_2Fe_4O_9$ impurity phase. Magnetic hysteresis loops with enhanced remnant magnetization and coercive field were obtained for the Gd-containing compounds. The improvement of magnetic behavior of the Gd-containing compounds is thought to arise mainly from the partial suppression of the spiral spin structure and the stronger interaction between magnetic ions. The magnetic transition temperatures of the compounds were found to be in the range 300^oC-310°C.

Dua *et al.* 2010 [48] synthesized the multiferroic $Bi_{1-x}La_xFeO_3$ (x = 0.0, 0.10, 0.20, 0.30) micro-particles by a hydrothermal technique. All the samples were phase pure crystallizing in a perovskite structure with a space group of R3c. The dielectric constant of $Bi_{1-x}La_xFeO_3$ sample increased after La doping, and reached the largest value for the sample of x = 0.20, both in low and high frequency range at room temperature. All the as-prepared samples exhibited magnetic moments starting above room temperature. It was found that the magnetic moment was significantly enhanced from 0.264 emu/g of $BiFeO_3$ to 0.658 emu/g of $Bi_{0.9}La_{0.1}FeO_3$ in a field of 3T at 77K.

Yan *et al.* 2010 [49] synthesis the $Bi_{1-x}La_xFeO_3$ (BLFO, x = 0.0–0.20) crystallites by the hydrothermal route. X-ray diffraction results indicate that pure BLFO crystallites could be obtained for $x \leq 0.10$, and the phase purity was sensitive to the PH value of precursor solutions. Transmission electron microscope observation reveals that needle like BLFO crystallites were formed for x = 0.10. The Neel temperature of BLFO crystallites for x = 0.1 shifts upwards, whereas the Curie temperature shifts downwards, compared with those of BFO crystallites without La substitution.

Khomchenko *et al.* 2010 [50] studied the crystal structure and multiferroic properties of polycrystalline $Bi_{1-x}Sm_xFeO_3$ ($0.16 < x < 6\ 0.20$) samples was performed by X-ray diffraction, piezoresponse force microscopy and SQUID-magnetometry techniques. It was reported that increasing samarium content induced a polar-to-no polar phase transition near x=0.2. Within the polar region, a rhombohedral and two orthorhombic modifications of $Bi_{1-x}Sm_xFeO_3$ were found.

But few reports are available on size dependent multiferroic properties of $BiFeO_3$. $BiFeO_3$ has been a focal point of research because, in bulk form, it is an antiferromagnetic, ferroelectric, and ferroelastic multiferroic material with electrical, magnetic, and structural ordering temperatures well above room temperature. The combined action of exchange and spin orbit interactions produces spin canting away from perfect antiferromagnetic ordering. The direction of the resulting small moment, however, rotates, superimposing a spiral spin arrangement with a wavelength of 62 nm, thereby producing a helimagnetic order and a vanishing magnetization in the bulk.

So, here we will work on synthesis of Gd doped $BiFeO_3$ nanoparticles and will explore its properties.

Chapter 3 Objectives and Methodology

3.1 Gaps in Research

From the review of literature, it has been found that the following areas are not much explored till now. Following are the gaps in the present study:

- Size-dependent multiferroic properties of Gd doped $BiFeO_3$ nanoparticles.

3.2 Objectives

- ✓ The synthesis of rare earth metal Gd doped $BiFeO_3$ nanoparticles by solution combustion synthesis method.
- ✓ The characterization of synthesized $BiFeO_3$ nanoparticles; structurally by X-ray diffraction (XRD), morphologically by Scanning Electron Microscopy (SEM), Transmission Electron Microscopy (TEM).
- ✓ The optical studies by Photoluminescence (PL).
- ✓ The electrical, dielectrics studies using respectively Polarization versus Electric field (PE) loop tracer,
- ✓ The thermal analysis of synthesized product done by Thermogravimetric analysis (TGA).

3.3 Methodology

Following steps will be taken to achieve the objectives:

- ❖ **Synthesis of Gd doped $BiFeO_3$nanoparticles:** The synthesis of rare earth metal-doped $BiFeO_3$ will be done by solution combustion method. In this method the equimolar solution of Bi $(NO_3)_3$ and Fe $(NO_3)_3$ are dissolved in de-ionized, and then glycine act as fuel added to above mixture of solution. Then the mixture is heated on hot plate for time till, the auto-ignition internally in solution will take place.
- ❖ **Structural Analysis:** The XRD characterization will be done to know about the crystal structure, crystallinity, and phase transformation with doping.

- **Morphological Characterization**: The morphology of the synthesized product will be examined by SEM and TEM.
- **Optical analysis:** The Photoluminescence (PL) analysis will be carried out to study optical transitions, defects in synthesized nanoparticles.
- **Electrical Characterization:** The PE loop tracer is used to study ferroelectric behavior of synthesized nanomaterials.
- **Magnetic measurements:** The VSM characterization will be performed to study the magnetic behavior of synthesized materials.
- **Thermal study:** To study the phase transition temperature the DSC/TGA will be done.

Synthesis of nano materials

The nano materials can be prepared by different method categorized viz. Bottom up and Top down

4.1 Top down approach

The **top-down** approach often uses the traditional workshop or micro fabrication methods where externally controlled tools are used to cut, mill and shape materials into the desired shape and order, micro patterning techniques, such as photolithography and inkjet belong to this category.

Some examples of top-down approach:

1. High energy milling
2. Chemical mechanical milling
3. Vapor phase condensation
4. Electro-explosion
5. Laser ablation
6. Sputtering

4.2 Bottom up approach

A bottom-up approach refers to the build-up of a material from the bottom i.e. atom by atom, molecule by molecule, or cluster by cluster. In crystal growth such as atoms, ions and molecules, after impinging onto the growth surface, assemble into crystal structure one after another. Although the bottom-up approach is nothing new, it plays an important role in the fabrication and processing of nanostructure and nanomaterials. There are several reasons for this. When structures fall into a nanomaterial scale, there is little choice for top-down approach .All the tools we have possessed are too big to deal with such tiny subjects. Bottom up approach also promises a better chance to obtain nanostructures with fewer defects, more homogeneous chemical composition and better short and long range ordering. This is bottom-up approach is driven

mainly by the reduction of Gibbs free energy, so that nanostructures and nanomaterials such produced are in a state closer to a thermodynamic equilibrium state. On the contrary, top-down approach most likely introduces internal stress, in addition to surface defects and contaminations. Nanolithography or nanomanipulation is commonly a bottom-up approach. Examples of bottom-up approach:

1. Solution combustion method
2. Sol-gel
3. Microemulsion
4. Reverse micelle
5. Chemical precipitation, etc.

4.3 Solution combustion method

Combustion synthesis has emerged as a facile and economically viable technique for the preparation of advanced ceramics, catalysts and nanomaterials. .

Combustion synthesis (CS) has emerged as an important technique for the synthesis and processing of advanced ceramics (structural and functional), catalysts, composites, alloys, intermetallics and nanomaterials. In CS, the exothermicity of the redox (reduction–oxidation nor electron transfer) chemical reaction is used to produce useful materials. Depending upon the nature of reactants: elements or compounds (solid, liquid or gas); and the exothermicity (adiabatic temperature, T), CS is described as: self-propagating high temperature synthesis (SHS); low-temperature combustion synthesis (LCS), solution combustion synthesis (SCS), gel-combustion, sol–gel combustion, emulsion combustion, volume combustion (thermal explosion), etc. Combustion synthesis processes are characterized by high-temperatures, fast heating rates and short reaction times.

These features make CS an attractive method for the manufacture of technologically useful materials at lower costs compared to conventional ceramic processes. Some other advantages of CS are:

(i)Use of relatively simple equipment
(ii)Formation of high-purity products

(iii)Stabilization of metastable phases and

(iv)Formation of virtually any size and shape products

4.4 Synthesis of Gd doped Nanoparticles of BiFeO3 by Solution /Auto-Combustion route

One of the most widely used and useful method of preparation of BFO is the combustion synthesis route using a fuel. The fuel used may be glycine, citric acid or urea. The process is based on the mixing of reactants that oxidize easily, such as metal nitrates, and an organic fuel, acting as a reducing agent. An external heat supply is needed to initiate the ignition of the mixture leading to a self-sustainment of an exothermic redox reaction. In this technique, based on the principles of the propellant chemistry, a thermally induced redox reaction takes place between an oxidant and a fuel. Many types of combustion synthesis exist which differ mainly in the physical state of the reactants or in the combustion modality. By combustion-based methods it is possible to produce monophasic nanopowders with homogeneous microstructure, at lower temperatures or shorter reaction times, if compared with other conventional methods like solid-state synthesis or nitrate method.

Bismuth ferrite was prepared by a novel combustion method using glycine as the fuel. The procedure adopted is

- Precursor was prepared in aqueous solution from metal nitrates and glycine. Solutions of Equimolar concentration of Bi $(NO_3)_3$ and Fe $(NO_3)_3$ were prepared. As Bi $(NO_3)_3$ is insoluble in Water, it was first dissolved in HNO_3. Furthermore the CTAB surfactant was used to capped And control the morphology and uniformity of product.
- Both these solutions were then properly mixed.
- Oxidized to fuel ratio was adjusted to 0.1.The appropriate amount of glycine was taken in other beaker and dissolved in appropriate amount of de-ionized then added to the above solution. The mixture was stirred until complete dissolution occurred.
- Then, the mixture of above solutions was heated and evaporated on a hot plate with stirring till It became a dark viscous resin. Continuous heating leads to the auto-ignition of dried resin with The evolution of large quantities of gases.
- The brownish color ash obtained after combustion was analyzed for perovskite-type $BiFeO_3$ phase.

• The whole process was over after 30 min, but the time between the actual ignition and the end of the reaction was less than 20 s.

• After the combustion is over in chamber, it is further heated for 5-10 minutes to allow complete combustion of material.

• After cooling, it is taken out of chamber and grinding is done to achieve finer powder.

• The powder was calcined at 450 C for 6 hour. Now the $BiFeO_3$ powder is ready for further characterization.

.

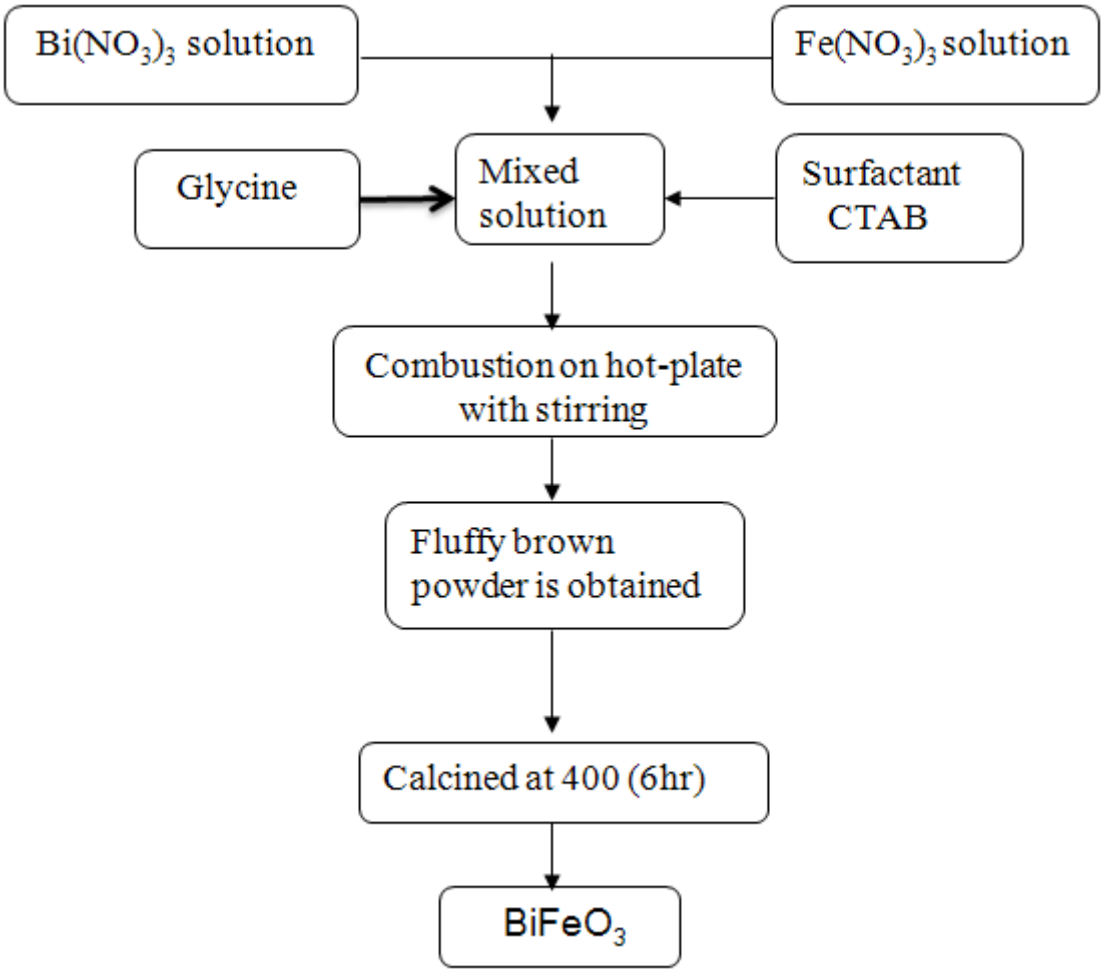

Figure 4.1: Various steps involve in synthesis of $BiFeO_3$

4.5 Safety conditions

The auto-combustion reaction can be explosive, yielding a high flame which quickly propagates

through the reactant mixture. Therefore, safety becomes more and more important when many grams of powder have to be prepared by auto-combustion synthesis, as observed by other authors. Moreover, if the combustion reaction is more explosive, more powder is displaced from the combustion beaker and the product is thus lost. Even if the combustion reaction takes place very calmly, without flame production, only 80% of the product can be recovered at low F/O ratios, because some of the very fluffy powder flies away with the combustion gases. At F/O = 0.8, where the intensity of the process is decreased, a 90% of recovery can be attained For these reasons, in this work, special care has been taken in the identification of the safety conditions. it is described that the combustion intensity decreases with F/O ratio and changes with the phase composition of the chemical mixture. Another important point is the material of the combustion beaker. On this respect, by comparing three combustion reactors made of different materials (sintered alumina,Pyrex glass and stainless steel) and by fixing all the other parameters, results show that sintered alumina reactor displays the highest combustion intensity, whereas stainless steel reactor displays the lowest one. This trend has been associated with the different dispersion capacity of the three materials. In summary, when this is possible, higher F/O ratios, lower pH values and combustion reactors with higher heat dispersion capacity are recommended in order to conduct safely the combustion.

4.6 Characterisation Techniques

The characterization of materials regarding determination of elemental composition, estimation of trace impurities, structural analysis, morphological analysis, dielectric analysis, magnetic analysis, identification of crystalline phases and information on crystal defects play an important role for the quality control and development of advanced materials and their use in precision devices. The nanostructures have been characterized by their structural, compositional, morphological, optical, magnetic and dielectric properties. The techniques include X-ray diffraction (XRD), Thermogravimetric analysis (TGA), Scanning electron microscopy (SEM), Transmission electron microscopy (TEM), Photoluminescence (PL) and Vibrational Sample Magnetometer (VSM)

4.6.1 X-ray diffraction

The X-ray diffraction (XRD) is a rapid analytical technique that reveals detailed information

about the chemical composition and crystallographic structure of natural and synthesized materials. The XRD is based on constructive interference of monochromatic X-rays and a crystalline sample. The interaction of the incident rays with the sample produces constructive interference (and a diffracted ray) when conditions satisfy: Bragg's Law, $n\lambda=2d \sin \theta$.This law relates the wavelength of electromagnetic radiation to the diffraction angle and the lattice spacing in a crystalline sample. These diffracted X-rays are then detected, processed and counted. By scanning the sample through a range of 2θ angles, all possible diffraction directions of the lattice should be attained due to the random orientation of the powdered material. Conversion of the diffraction peaks to d-spacings allows identification of the mineral because each mineral has a set of unique d-spacings. Typically, this is achieved by comparison of d-spacings with standard reference patterns. All diffraction methods are based on generation of X-rays in an X-ray tube.

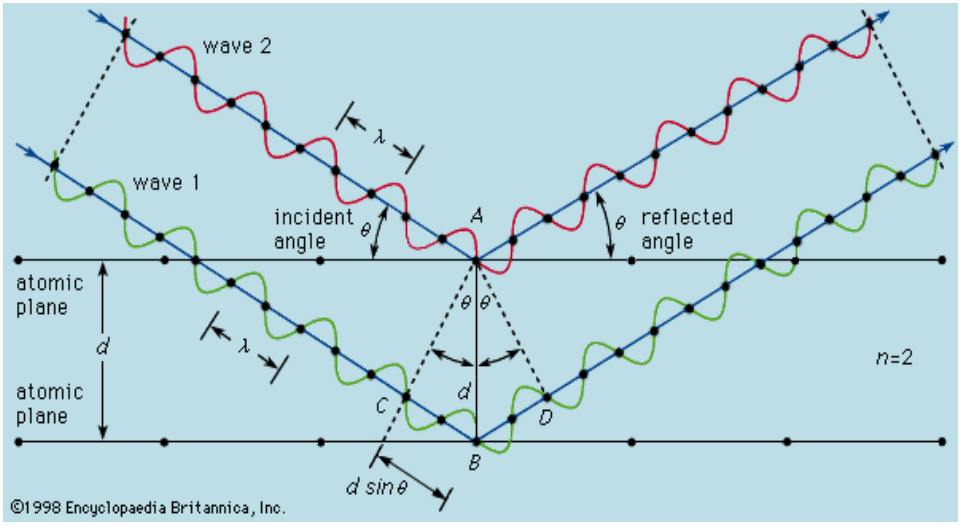

Figure 4.2: The Bragg's law reflection, the diffracted x-rays exhibit costructive interference when the distance between paths ABC and AB'C' differs by an integer number of wavelengths (λ).

These X-rays are directed at the sample, and the diffracted rays are collected. A key component of all diffraction is the angle between the incident and diffracted rays. The geometry of an X-ray diffractometer is such that the sample rotates in the path of the collimated X-ray beam at an angle θ while the X-ray detector is mounted on an arm to collect the diffracted X-rays and rotates at an angle of 2θ.

Applications

- Identification of unknown crystalline materials.
- Find the crystal structure of an unknown material.
- To find crystallite size.

4.6.2 Thermogravimetric analysis

Thermogravimetric analysis (TGA) is a thermal analysis technique which measures the weight change in a material as a function of temperature and time, in a controlled environment. This can be very useful to investigate the thermal stability of a material, or to investigate its behavior in different atmospheres (e.g. inert or oxidizing). A derivative weight loss curve can identify the point where weight loss is most apparent.

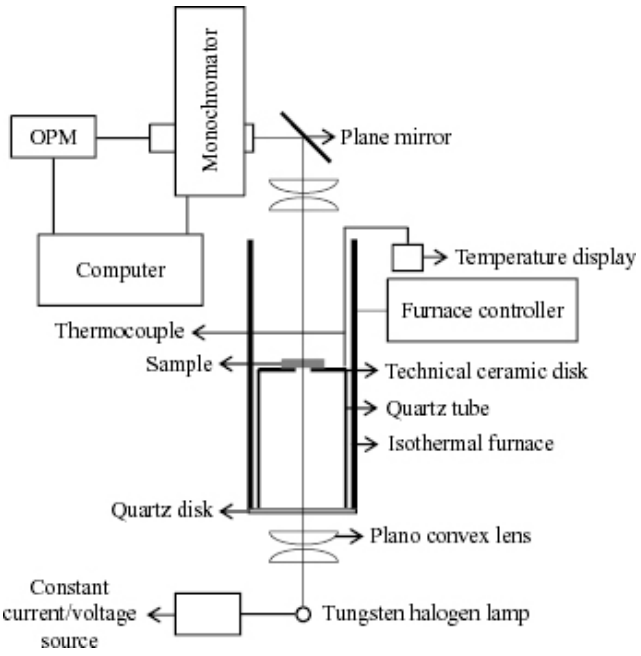

Figure 4.3: Schematic of TGA/DTA

TGA is commonly employed in research and testing to determine characteristics of materials such as polymers, to determine degradation temperatures, absorbed moisture content of materials, the level of inorganic and organic components in materials, decomposition points

of explosives, and solvent residues. It is also often used to estimate the corrosion kinetics in high temperature oxidation. Simultaneous TGA-DTA/DSC measures both heat flow and weight changes (TGA) in a material as a function of temperature or time in a controlled atmosphere. Simultaneous measurement of these two material properties not only improves productivity but also simplifies interpretation of the results.

Uses of TGA/DTA:

- Thermal stability/degradation investigation of organic or inorganic materials, e.g. polymers, composites, glasses, metals, minerals etc.
- Thermal stability/degradation investigations in inert or oxidative atmospheres, or in vacuum
- Determination of organic/inorganic content of mixtures
- Phase transition measurement (e.g. glass transition, clustering, crystallinity, melting point)

4.6.3 Scanning Electron Microscope

Scanning Electron Microscope (SEM) is a type of electron microscope that images a sample by scanning it with a high-energy beam of electrons in a raster scan pattern. The electrons interact with the atoms that make up the sample producing signals that contain information about the sample's surface topography, composition, and other properties such as electrical conductivity.

Electron bombardment of a sample is unique to microprobe analysis and produces a large number of effects from the target material (Figure 4.6). The incident electrons interact with specimen atoms and are significantly scattered by them (rather than penetrating the sample in a linear fashion). Most of the energy of an electron beam will eventually end up heating the sample (phonon excitation of the atomic lattice); however, before the electrons come to rest, they undergo two types of scattering: elastic and inelastic. In elastic scattering, the electron trajectory changes, but its kinetic energy and velocity remain essentially constant (due to large differences between the mass of the electron and nucleus). This process is known as electron backscattering .In inelastic scattering, the trajectory of the incident electron is only slightly perturbed, but

energy is lost through interactions with the orbital electrons of the atoms in the specimen. Inelastic interactions produce diverse effect including:

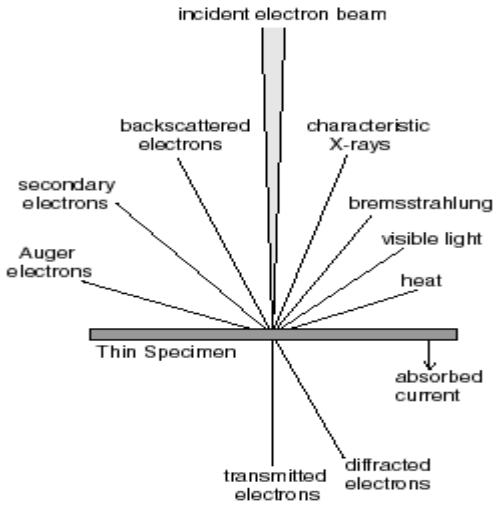

Figure 4.4: Interaction of electron with matter

- phonon excitation (heating)
- cathodoluminescence (visible light fluorescence)
- continuum radiation (bremsstrahlung or "braking" radiation)
- characteristic x-ray radiation
- plasmon production (secondary electrons)
- Auger electron production (ejection of outer shell electrons)

SEM uses a focused beam of high-energy electrons to generate a variety of signals at the surface of solid specimens. The signals that derive from electron-sample interactions reveal information about the sample including external morphology (texture), chemical composition, and crystalline structure and orientation of materials making up the sample. Accelerated electrons in an SEM carry significant amounts of kinetic energy, and this energy is dissipated as a variety of signals produced by electron-sample interactions when the incident electrons are decelerated in the solid sample. These signals include secondary electrons (that produce SEM images), backscattered electrons (BSE), diffracted backscattered electrons (EBSD that are used to determine crystal structures and orientations of minerals), photons (characteristic X-rays that are used for elemental analysis and continuum X-rays), visible light. Secondary electrons and backscattered

electrons are commonly used for imaging samples: secondary electrons are most valuable for showing morphology and topography on samples and backscattered electrons are most valuable for illustrating contrasts in composition in multiphase samples (i.e. for rapid phase discrimination).

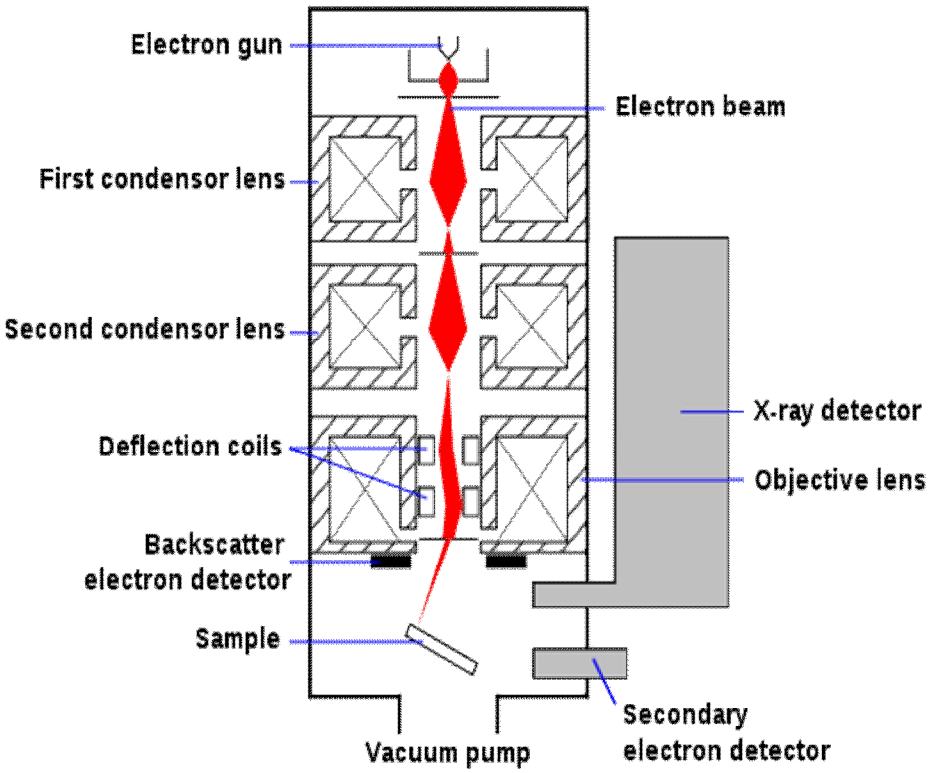

Figure 4.5: Schematic of different component of SEM

Applications

- To study morphology of synthesized product.
- Acquiring elemental maps or spot chemical analyses using EDS.
- Discrimination of phases based on mean atomic number.
- To identify phases based on qualitative chemical analysis and/or crystalline structure.
- SEMs equipped with diffracted backscattered electron detectors (EBSD) can be used to examine micro fabric and crystallographic orientation in many materials.

4.6.4 Transmission electron microscopy

Transmission electron microscopy (TEM) is a microscopy technique whereby a beam of electrons is transmitted through an ultra thin specimen, interacting with the specimen as it passes through. An image is formed from the interaction of the electrons transmitted through the specimen; the image is magnified and focused onto an imaging device, such as a fluorescent screen, on a layer of photographic film, or to be detected by a sensor such as a CCD camera. TEMs are capable of imaging at a significantly higher resolution than light microscopes, owing to the small de Broglie wavelength of electrons. At smaller magnifications TEM image contrast is due to absorption of electrons in the material, due to the thickness and composition of the material.

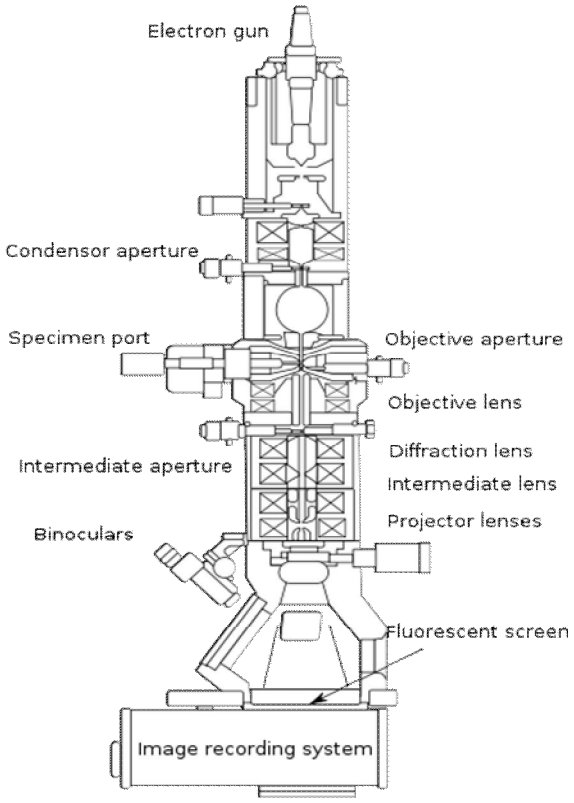

Figure 4.6: Schematic of TEM

At higher magnifications complex wave interactions modulate the intensity of the image, requiring expert analysis of observed images. Alternate modes allow TEM to observe modulations in chemical identity, crystal orientation, and electronic structure

Applications

- Morphological analysis, Electronic diffraction, X-EDS qualitative and semi-quantitative analysis, either in Spot or in Semi Stem mode.

4.6.5 Photoluminescence

All solids, including semiconductors have so-called “energy gaps” for the conducting electrons. If a light particle (photon) has energy greater than the band gap energy, then it can be absorbed and thereby raise an electron from the valence band up to the conduction band across the forbidden energy gap. In this process of photo excitation, the electron generally has excess energy which it loses before coming to rest at the lowest energy in conduction band. At this point the electron eventually falls back into a luminescent photon which is emitted from the material.

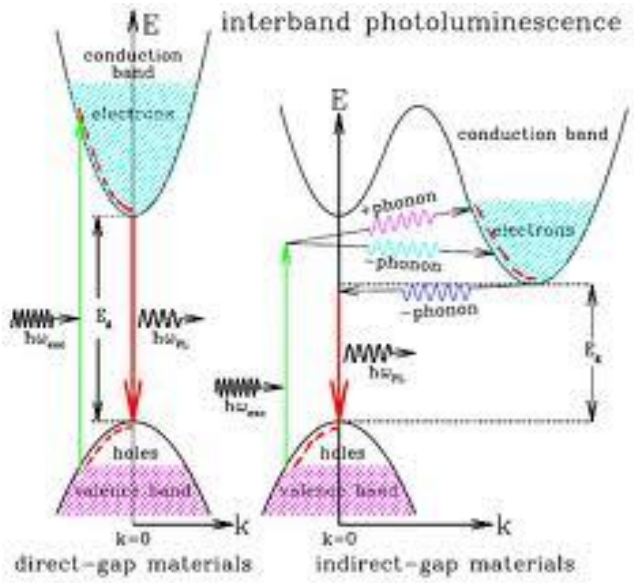

Figure 4.7: Different transitions involve in sample

Thus the energy of the emitted photon is a direct measure of the band gap energy, E_g. The process of photon excitation followed by photon emission called photoluminescence. The PL spectrum provides the transition energies, which can be used to determine electronic energy levels. The PL intensity gives a measure of the relative rates of radiative and non-radiative recombination. Variation of the PL intensity with external parameters like temperature and applied voltage can

be used to characterize further the underlying electronic states and bands. The simplest photoluminescent processes are resonant radiations, in which a photon of a particular wavelength is absorbed and an equivalent photon is immediately emitted.

Uses of PL

- Band Gap Determination
- Impurity Levels and Defect Detection.
- Recombination Mechanisms
- Material Quality

4.6.6 Vibrating sample magnetometer

A vibrating sample magnetometer (VSM) is a scientific instrument that is used relatively widespread for magnetic measurements. If a sample of any material is placed in a uniform magnetic field, created between the poles of an electromagnet, a dipole moment will be induced. If the sample vibrates with sinusoidal motion a sinusoidal electrical signal can be induced in suitable placed pick-up coils. The signal has the same frequency of vibration and its amplitude will be proportional to the magnetic moment, amplitude, and relative position with respect to the pick-up coils system.

The sample is fixed to a small sample holder located at the end of a sample rod mounted in an electromechanical transducer

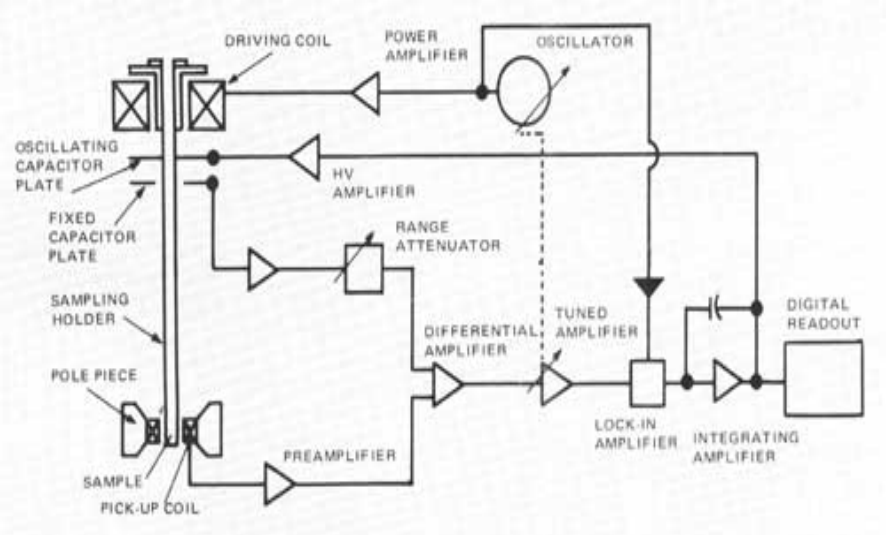

Figure 4.8: Schematic of different components of VSM

The transducer is driven by a power amplifier which itself is driven by an oscillator at a frequency of 90 Hertz. So, the sample vibrates along the Z axis perpendicular to the magnetizing field. The latter induced a signal in the pick-up coil system that is fed to a differential amplifier. The output of the differential amplifier is subsequently fed into a tuned amplifier and an internal lock-in amplifier that receives a reference signal supplied by the oscillator. The output of this lock-in amplifier, or the output of the magnetometer itself, is a DC signal proportional to the magnetic moment of the sample being studied.

With the help of vibrating sample magnetometer one can measure the DC magnetic moment as a function of temperature, magnetic field, angle and time. So, it helps in susceptibility and magnetization studies. The most common measurements done are: hysteresis loops, susceptibility or saturation magnetization as a function of temperature (thermo magnetic analysis), magnetization curves as a function of angle (anisotropy) and magnetization as a function of time.

5.1 Structural and phase analysis

XRD patterns of as synthesized $BiFeO_3$, $Bi_{0.98}Gd_{0.02}FeO_3$, $Bi_{0.96}Gd_{0.04}FeO_3$, $Bi_{0.94}Gd_{0.06}FeO_3$ shown in figure 5.1. All the peaks are indexed and well matched to rhombohedral structure with hexagonal phase with lattice parameter a = 3.952 Å (File No. 722112). The XRD pattern of Gd doped BFO show an additional peak around 28.035 which is due to formation of $BiGd_2Fe_5O_{12}$ phase (File No. 480231).

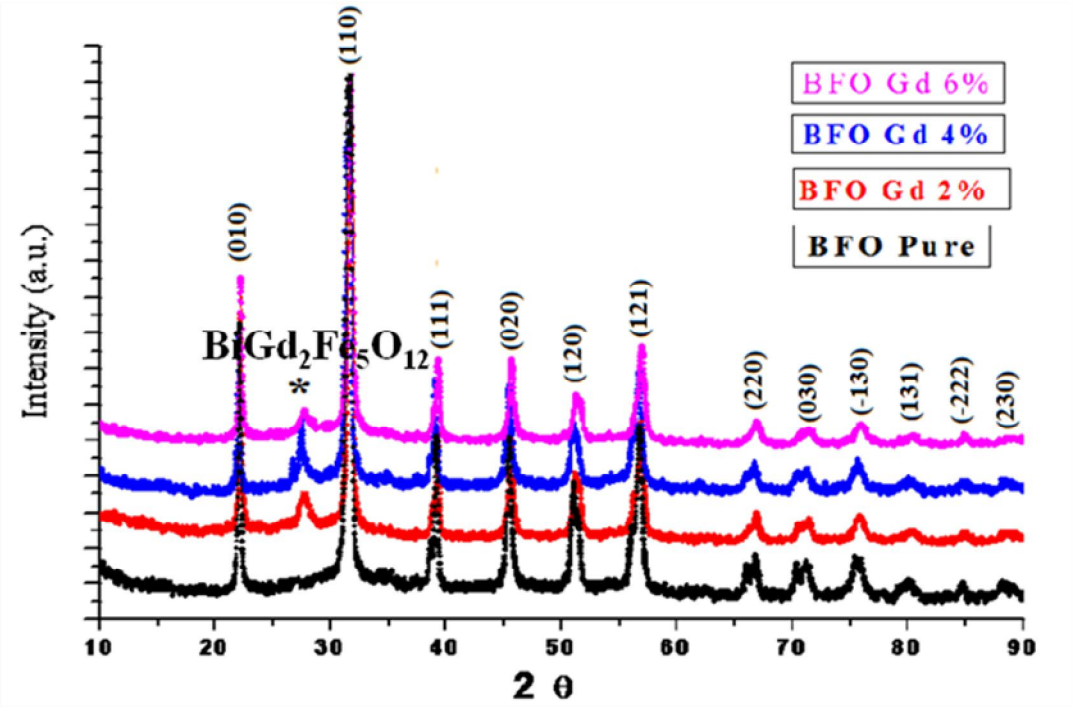

Figure 5.1: XRD pattern of pure $BiFeO_3$ and Gd doped $BiFeO_3$ nanoparticles

The crystallite sized of both calcined and as synthesized samples calculated using Hall-Williamson method and Debye Scherer's equation

$$B \cdot \cos(\theta) = \frac{k\lambda}{D} + \eta \cdot \sin(\theta),$$

The value of η is the strain in the crystallites, B is full width at half maxima (FWHM) the value of D represents the size of the crystallites. The constant k is typically close to unity and ranges

From 0.8-1.39. when we plot $B \cdot \cos(\theta)$ vs. $\sin(\theta)$ we get a straight line with slope η and intercept $\frac{k\lambda}{D}$. The variation crystallites size with Gd doping and calcinations at 450^0C are shown in figure 5.2. It is clear from the figure 5.2 that for as synthesized $BiFeO_3$ nanoparticles the crystallites size increase Gd doping.

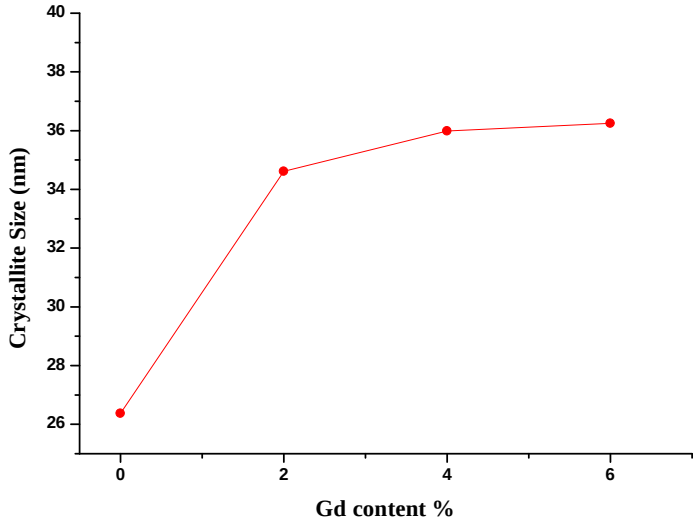

Figure 5.2: The variation crystallites size with Gd doping

5.2Thermal analysis

The thermal behavior of samples is observed by TGA, the TGA curve of the as prepared pure Bi samples is shown in figure 5.3.

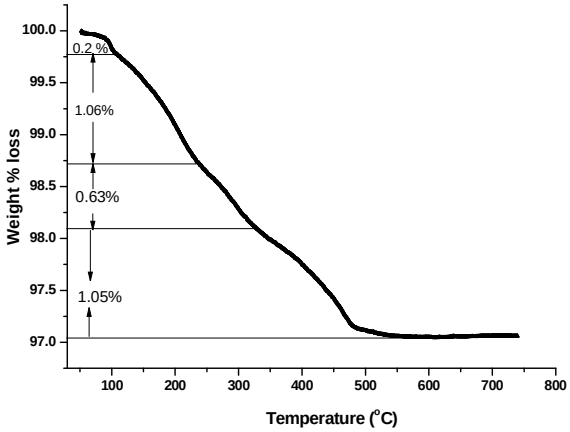

Figure 5.3: TGA curve of as synthesized product

Since the glycine can form different chelate compounds with Bi^{3+} and Fe^{3+} ions, different behavior was observed from curves.

5.3 SEM study

SEM micrographs of pure and 6% Gd doped $BiFeO_3$ pellets calcined at 800^0C is shown in figure 5.4.

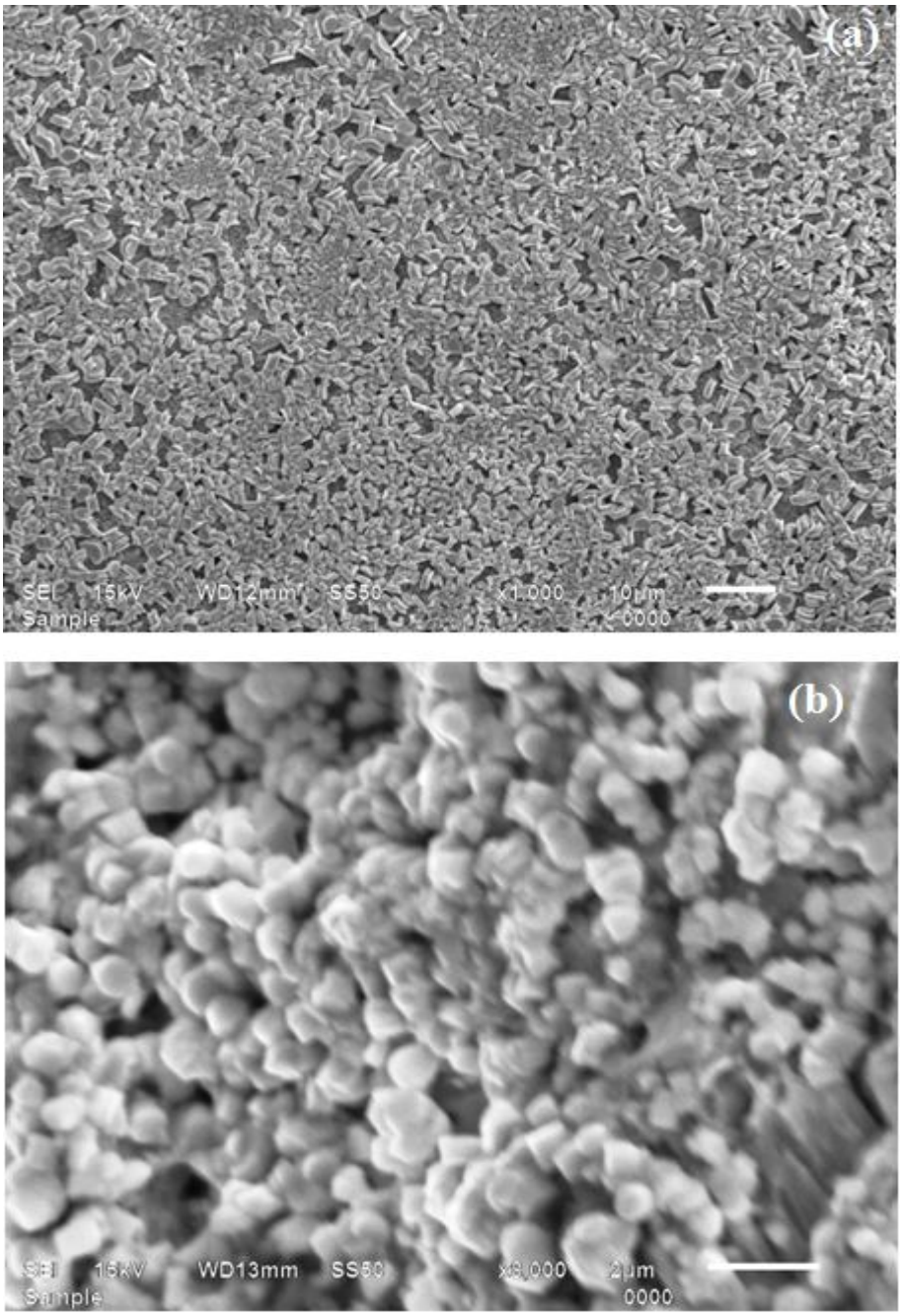

Figure 5.4: SEM micrographs of (a) pure and (b) 6% Gd doped $BiFeO_3$

The morphology of pure $BiFeO_3$ particles seemed to be approximately dumb-bell in shape. But however with 6% Gd doping leads to particles nearly spherical in shape with grain size 200nm. In both cases, particles are agglomerated and a high interconnection of the grains can be seen.

5.4 TEM Study

The morphology of as synthesized $BiFeO_3$ nanoparticles was examined on TEM as shown in figure 5.5.

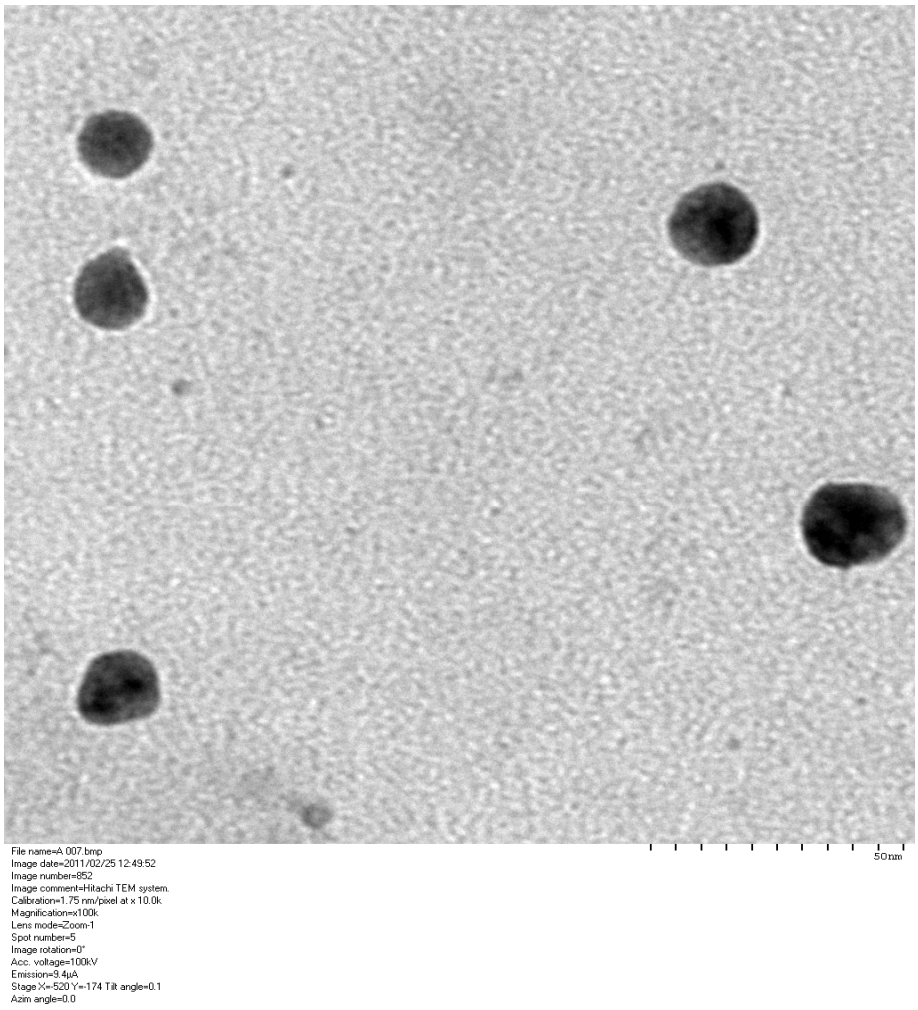

Figure 5.5: TEM micrograph of pure $BiFeO_3$ nanoparticles.

It is clear that particles are spherical in shape with average particle size ~17 nm. Hardly any aggregation could be found in our samples.

5.5 Photoluminescence Study

Figure 5.6 shows the PL spectra of pure and Gd doped $BiFeO_3$ nanoparticles. It is clear from the figure 5.4 that for pure $BiFeO_3$ nanoparticles a strong blue emission around 454 nm is observed which is attributed to the self-activated center. But with addition of Gd in $BiFeO_3$ another strong green emission at 548 nm and 558 nm is observed for 2% and 4, 6 % doping.

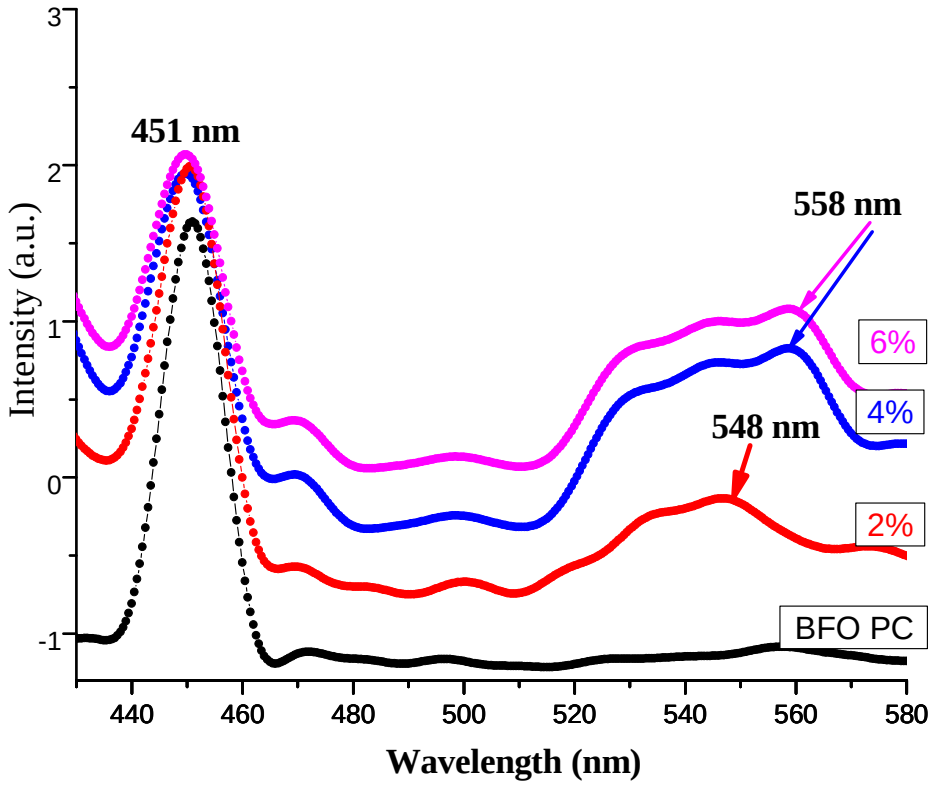

Figure 5.6: PL spectra of pure $BiFeO_3$ nanoparticles and Gd doped $BiFeO_3$ nanoparticles.

The light emission in attributed to Gd^{2+} centre, and ascribe to the transition $5d^1$ and $4f^7$ electrons in Gd^{2+}. The luminescence centers of Gd^{2+} ions make amount of electron-hole pairs, which recombine immediately and emit more photons.

5.6 Magnetic study

The magnetic study of pure and 6% Gd doped $BiFeO_3$ nanoparticles are shown in figure 5.7. It is clear from the MH curves that pure $BiFeO_3$ nanoparticles are showing antiferromagnetic. The magnetic study of pure and 6% Gd doped $BiFeO_3$ nanoparticles are shown in figure 5.7. It is clear from the MH curves that pure $BiFeO_3$ nanoparticles are showing antiferromagnetic

behaviour as such no saturation in MH curve is observed, also the area under the curve is also very negligible. But however it also clear from the figure 5.7 that with addition of 6% of Gd in $BiFeO_3$ they show ferromagnetic behaviour. It is well known that Gd is ferromagnetic in nature; also the size of $BiFeO_3$ nanoparticles is 22 nm (figure 5.5). So due to ferromagnetic nature and splitting of spin spiral structure of $BifeO_3$ (spin spiral structure is observed with period of 62 nm) with size may be responsible for the observed ferromagnetic nature of Gd doped $BiFeO_3$.

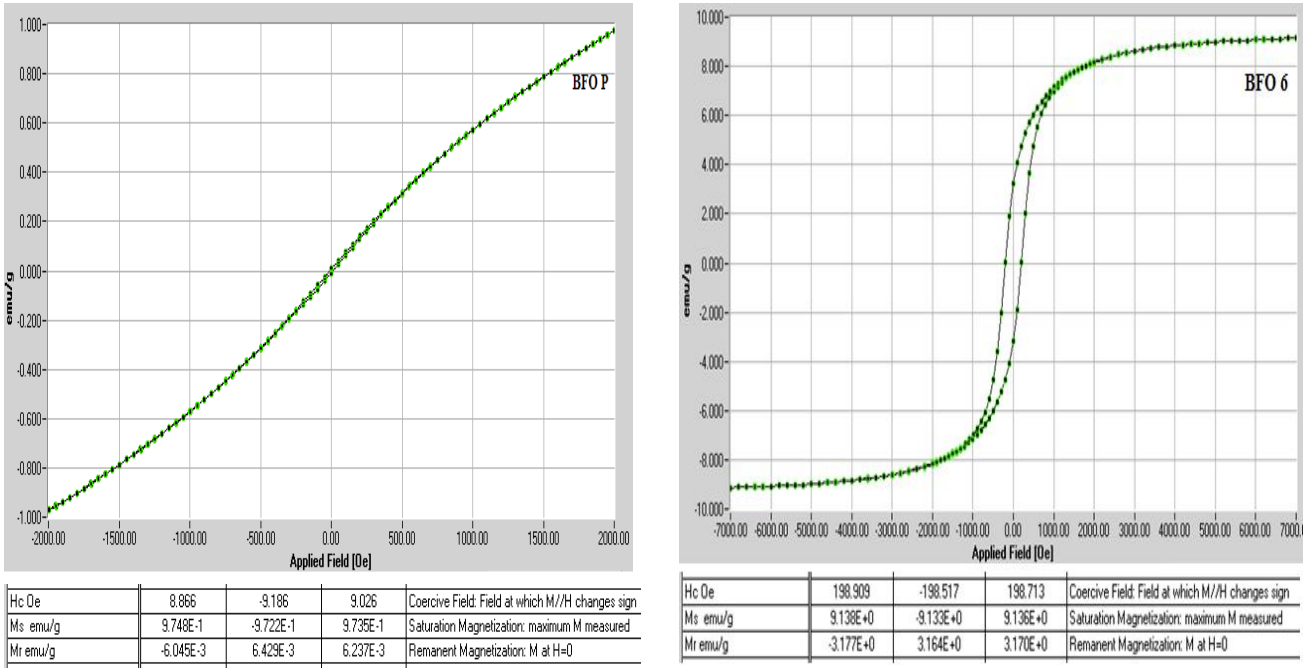

Hc Oe	8.866	-9.186	9.026	Coercive Field: Field at which M//H changes sign
Ms emu/g	9.748E-1	-9.722E-1	9.735E-1	Saturation Magnetization: maximum M measured
Mr emu/g	-6.045E-3	6.429E-3	6.237E-3	Remanent Magnetization: M at H=0

Hc Oe	198.909	-198.517	198.713	Coercive Field: Field at which M//H changes sign
Ms emu/g	9.138E+0	-9.133E+0	9.136E+0	Saturation Magnetization: maximum M measured
Mr emu/g	-3.177E+0	3.164E+0	3.170E+0	Remanent Magnetization: M at H=0

Figure 5.7: MH hysteresis loop of pure and 6 % Gd doped $BiFeO_3$ nanoparticles.

5.7 Ferroelectric study

To study the ferroelectric behaviour of pure and 6% Gd doped $BiFeO_3$, polarization as function of electric field (P-E) measurements were carried out at room temperature as shown figure 5.8. It is observed that, a weak ferroelectric loop was observed in case of pure $BiFeO_3$ ceramics system. With increasing the concentration of Gd the saturation polarization value increases significantly from 1 to 65 $\mu C/cm^2$, at room temperature exhibiting the contribution of Bi rich ions for the

enhancement of ferroelectric properties with respect to its original undoped $BiFeO_3$. The 6% Gd doped $BiFeO_3$ show elliptical P-E loop.

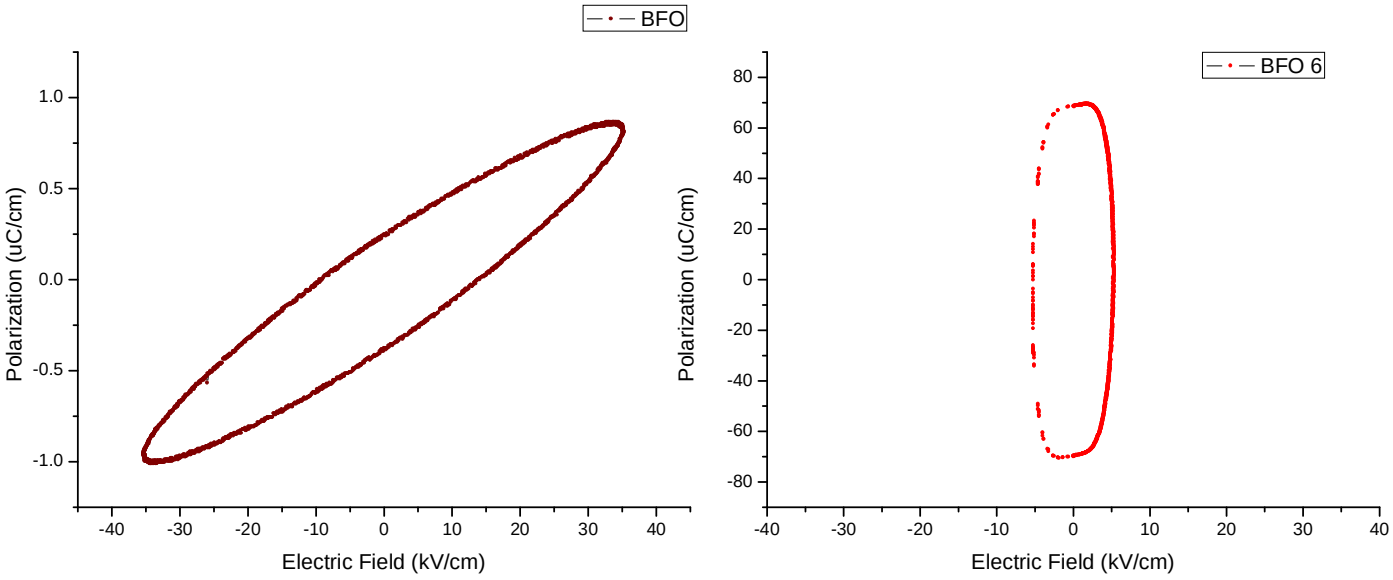

Figure 5.8 P-E hysteresis loop of pure and 6% Gd doped $BiFeO_3$

5.8 Conclusions

The aim of the present work was to investigate, the effect of size and Gd doping in $BiFeO_3$ nanoparticles on structural, magnetic, ferroelectric and morphological properties.

- Synthesis of pure and Gd doped $BiFeO_3$ nanoparticles have been done by solution combustion method using glycine as fuel.

- All the peaks are indexed and well matched to rhombohedral structure with hexagonal phase with lattice parameter a = 3.952 Å (File No. 722112). The XRD pattern of Gd doped BFO show an additional peak around 28.035 which is due to formation of $BiGd_2Fe_5O_{12}$ phase. The average crystallite size found to be increase with Gd doping in host $BiFeO_3$.

- The morphology of pellets of pure $BiFeO_3$ and 6% Gd doped $BiFeO_3$ calcined at 800^0 C shows that pure $BiFeO_3$ particles seemed to be approximately dumb-bell in shape. But however with 6% Gd doping leads to particles nearly spherical in shape with grain size 200nm. In both cases, particles are agglomerated and a high interconnection of the grains can be seen.

- TEM study reveals that, as synthesized nanoparticles are spherical in shape with average particle size ~17 nm. Also, no aggregation had been found.

- PL spectra of pure and Gd doped $BiFeO_3$ nanoparticles give a strong blue emission around 454 nm is observed which is attributed to the self-activated center. But with addition of Gd in $BiFeO_3$ another strong green emission at 548 nm and 558 nm is observed for 2% and 4, 6 % doping. The light emission in attributed to Gd^{2+} centre, and ascribe to the transition $5d^1$ and $4f^7$ electrons in Gd^{2+}. The luminescence centers of Gd^{2+} ions make amount of electron-hole pairs, which recombine immediately and emit more photons

- Magnetic study reveals that, M-H curves of pure $BiFeO_3$ nanoparticles are showing antiferromagnetic behaviour, as no saturation in M-H curve is observed; also the area under the curve is also very negligible. But however with addition of 6% of Gd in

$BiFeO_3$ they show ferromagnetic behaviour. It is well known that Gd is ferromagnetic in nature; also the size of $BiFeO_3$ nanoparticles is 22 nm. So due to ferromagnetic nature and splitting of spin spiral structure of $BifeO_3$ (spin spiral structure is observed with period of 62 nm) with size may be responsible for the observed ferromagnetic nature of Gd doped $BiFeO_3$.

- To study the ferroelectric behaviour of pure and 6% Gd doped $BiFeO_3$, polarization as function of electric field (P-E) measurements were carried out at room temperature. It is observed that, a weak ferroelectric loop was observed in case of pure $BiFeO_3$ ceramics system. By increasing the concentration of Gd the saturation polarization value increases significantly from 1 to 65 $\mu C/cm^2$, at room temperature exhibiting the contribution of Bi rich ions for the enhancement of ferroelectric properties with respect to its original undoped $BiFeO_3$. The 6% Gd doped $BiFeO_3$ show elliptical P-E loop

References

[1] N Lane, J. Nano. Res. 3 (2001) 95.

[2] R F Service Science 290 (2000) 1526.

[3] Schmid, H. Ferroelectrics 162, (1994) 665.

[4] Y Wang, J Hu, Y Lin, C W Nan, NPG Asia Mater. 2 (2010) 61.

[5] N A Hill, J. Phys. Chem. B 104 (2000) 6694.

[6] C Ederer, N A Spaldin, Phys. Rev. B 71 (2005) 224103.

[7] I Sosnowska, T P Neumaier, E Steichele, J. Phys. C: Solid State Phys.15 (1982) 4835.

[8] P Curie, J de Physique 3 (1894) 393.

[9] D N Astov, Sov. Phys. JETP 11 (1960) 708.

[10] G T Rado, V J Folen, Phys. Rev. Lett. 7 (1961) 310.

[11] G A Smolensky, A I Agranovskaya, V A Isupov, Sov. Phys. Solid State 1 (1959) 149.

[12]V E Wood, A E Austin, Int. J. Magn. 5 (1973) 303.

[13] L W Martin, Y H Chu, R Ramesh Mater. Sci. Engg. R 68 (2010) 89.

[14] S K Pradhan, J Das, P P Rout, S K Das, D K Mishra, D R Sahu, A K Pradhan, V V Srinivasu, B B Nayak, S Verma , B K Roul, J. Magn. Mag. Mater. 322 (2010) 3614.

[15] J Wang, M Y Li, X L Liu, L Pei, J Liu, B F Yu, X Z Zhao 55 (2010) 1594.

[16] I Sonowska, T Peterlin-Neumaier, E Stelchele, J. Phys. C 15 (1982) 4835.

[17] J.R. Teague, R. Gerson, W.J. James, Solid State Commun. 8 (1970) 1073.

[18] F Kubel, H Schmid, Acta Crystallogr. B46 (1990) 698.

[19] P Royen, K Swars, Angew Chem 24 (1957) 779.

[20] R Ramesh, Nature 46 (2009) 129.

[21] S V Kiselev, R P Ozerov, G S Zhdanov, Sov Phys Dokl 7 (1963) 742.

[22] J R Teague, R Gerson, W J James, Solid State. Commun. 8 (1963) 1073.

[23] C Michel, J M Moreau, G D Achenbach, R Gerson, W J James, Solid State Commun. 7 (1969) 701.

[24] J M Moreau, C Michel, R Gerson, W J James, J Phys Chem Solids 32 (1971) 1315.

[25] P Fischer, M Polomska, I Sosnowska, M Szymanski, J Phys. C 13 (1980) 1931.

[26] M S Kartavtseva, O Y Gorbenko, A R Kaul, T V Murzina, Thin Solid Films 518 (2010) 4750.

[27] I E Dzyaloshinskii, Sov Phys JETP 5 (1957) 1259.

[28] N A Hill, Annu. Rev. Mater. Res. 32 (2002) 1.

[29] J Wang, J B Neaton, H Zheng, V Nagarajan, S B Ogale, B Liu, D Viehland, V Vaithyanathan, D G Schlom, U V Waghmare, N A Spaldin, K M Rabe, M Wuttig, R Ramesh, Science 299 (2003) 1719.

[30] W Eerenstein, N D Mathur, J F Scott, Nature 17 (2006) 442.

[31] CNR Rao, C R Serrao, J. Mater. Chem. 17 (2007) 4931.

[32] C A F Vaz, J Hoffman, C H Ahn, R Ramesh , Adv. Mater. (2010) 2900.

[33] G Catalan, J F Scott, Adv. Mater. 21 (2009) 2463.

[34] V L Mathe, K K Patankar, M B Kothalei, S B Kulkarni, P B Joshi, S A Patil, Indian Academy of Sciences Journal of Physics 58 (2009) 1105

[35] V R Palkar, C Darshan, Kundaliya, S K Malik, S Bhattacharya, Physical Review B 69 (2004) 212102.

[36] A K Pradhan, K Zhang, D Hunter, J B Dadson, G B Loutts, J Appl. Phys. 97 (2005) 093903

[37] J K Kim, S S Kim, W J Kim, Materials Letters 59 (2005) 4006.

[38] D H Wang, W C Goh, M Ning, C K Ong, Appl. Phys. Let. 88 (2006) 212907.

[39] C Fanggao, S Guili, F Kun, Q Ping, Z Qijun, J Rare Earths 24 (2006) 143.

[40] V A Khomchenko, D A Kiselev, J M Vieira, A L. Kholkin, Appl. Phys. Lett. 90 (2007) 242901.

[41] S R Das, R N P Choudhary, P Bhattacharya, R S Katiyar, Appl. Phys. Let. 101 (2007) 034104.

[42] W N Su, D H Wang, Q Q Cao, Z D Han, J Yin, J R Zhang, Y W Du, Appl. Phys. Let. 91 (2007) 092905.

[43] M Thrall, R Freer, C Martin, F Azougha, B Patterson, R J Cernik, J Euro. Cera. Soc. 28 (2008) 2567.

[44] V A Khomchenko, D A Kiselev, I K Bdikin, V V Shvartsman, P Borisov, W Kleemann, J M Vieira, A L Kholkin, Appl. Phys. Lett. 93 (2008) 262905.

[45]V R Reddy, D Kothari, A Gupta, S M Gupta, Appl.Phys. let. 94 (2009) 082505.

[46]VA Khomchenko, VV Shvartsman, P Borisov, W Kleemann, D A Kiselev, I K Bdikin, J M Vieira, A L Kholkin, Acta Materialia 57 (2009) 5137.

[47]A Z Simoesa, F G Garcia, C S Riccardi, Mat.Chem. Phys. 116 (2009) 305.

[48]M Al-Haj Cryst. Res. Technol. 45 (2010) 89.

[49]Y Dua, Z X Chenga, M Shahbazia, E W Collingsb, S X Doua, X L Wanga, J. Alloys Comp.490 (2010) 641.

[50] X Yan, J Chen, Y Qi, J Cheng, Z Meng, J Euro. Cera. Soc. 30 (2010) 265.